Atmos. Meas. Tech. Discuss., 8, 10179–10211, 2015
www.atmos-meas-tech-discuss.net/8/10179/2015/
doi:10.5194/amtd-8-10179-2015

Atmospheric Measurement Techniques Discussions
Open Access

Modeling the Zeeman effect in high altitude SSMIS channels for numerical weather prediction profiles: comparing a fast model and a line-by-line model

R. Larsson[1], M. Milz[1], P. Rayer[2], R. Saunders[2], W. Bell[2], A. Booton[2], S. A. Buehler[3], P. Eriksson[4], and V. John[5]

[1]Luleå University of Technology, Department of Computer Science, Electrical and Space Engineering, Kiruna, Sweden
[2]Met Office, Exeter, UK
[3]University of Hamburg, Meteorological Institute, Hamburg, Germany
[4]Chalmers University of Technology, Department of Earth and Space Sciences, Gothenburg, Sweden
[5]EUMETSAT, Darmstadt, Germany

Received: 9 June 2015 – Accepted: 2 September 2015 – Published: 2 October 2015

Correspondence to: R. Larsson (ric.larsson@gmail.com)

Published by Copernicus Publications on behalf of the European Geosciences Union.

Abstract

We present a comparison of a reference and a fast radiative transfer model using numerical weather prediction profiles for the Zeeman-affected high altitude Special Sensor Microwave Imager/Sounder channels 19–22. We find that the models agree well for channels 21 and 22 compared to the channels' system noise temperatures (1.9 and 1.3 K, respectively) and the expected profile errors at the affected altitudes (estimated to be around 5 K). For channel 22 there is a 0.5 K average difference between the models, with a standard deviation of 0.24 K for the full set of atmospheric profiles. Same channel, there is 1.2 K in average between the fast model and the sensor measurement, with 1.4 K standard deviation. For channel 21 there is a 0.9 K average difference between the models, with a standard deviation of 0.56 K. Same channel, there is 1.3 K in average between the fast model and the sensor measurement, with 2.4 K standard deviation. We consider the relatively small model differences as a validation of the fast Zeeman effect scheme for these channels. Both channels 19 and 20 have smaller average differences between the models (at below 0.2 K) and smaller standard deviations (at below 0.4 K) when both models use a two-dimensional magnetic field profile. However, when the reference model is switched to using a full three-dimensional magnetic field profile, the standard deviation to the fast model is increased to almost 2 K due to viewing geometry dependencies causing up to ±7 K differences near the equator. The average differences between the two models remain small despite changing magnetic field configurations. We are unable to compare channels 19 and 20 to sensor measurements due to limited altitude range of the numerical weather prediction profiles. We recommended that numerical weather prediction software using the fast model takes the available fast Zeeman scheme into account for data assimilation of the affected sensor channels to better constrain the upper atmospheric temperatures.

AMTD
8, 10179–10211, 2015

1 Introduction

The main isotopologue of molecular oxygen's ground state millimeter wavelength band around 60 GHz is used by several satellites to remotely measure temperature. This is because the band's radiometric signal is strong due to molecular oxygen's high and fairly constant volume mixing ratio (~ 21 %) at all altitudes below about 80 km (see e.g. Anderson et al., 1986, for the O_2 volume mixing ratio in the US standard atmosphere). Some examples of sensors utilizing this band for temperature soundings are the Advanced Microwave Sounder Unit (AMSU-A), the Special Sensor Microwave Imager/Sounder (SSMIS; Kunkee et al., 2008), and the Microwave Limb Sounder (MLS; Schwartz et al., 2006). All the lines of the millimeter band experience magnetic splitting and polarization from the Zeeman effect (Zeeman, 1897; Lenoir, 1967, 1968). In the atmosphere of Earth, this magnetic splitting is larger than the Doppler broadening, but only at higher altitudes is the magnetic splitting larger than the pressure broadening. As a simplistic and intuitive guideline for Earth, Doppler broadening in the 60 GHz band is about 50–70 kHz, magnetic splitting is in the range of 0.5–2 MHz, and pressure broadening by air is in the range of 10–20 kHz Pa^{-1} (see e.g. Rothman et al., 2013, for air pressure broadening). Measured signals with significant weight at altitudes above what corresponds to 25–200 Pa are therefore altered by magnetism. As a comparison, numerical weather prediction schemes usually profile up to 2–10 Pa. The Zeeman effect must thus be taken into account by the radiative transfer schemes used as forward models for numerical weather prediction assimilations at the top of the modeled profiles. This has been pointed out by Lenoir (1967, 1968); Liebe (1981); Rosenkranz and Staelin (1988); Hartmann et al. (1996); Han et al. (2007); Kobayashi et al. (2009), and Stähli et al. (2013), among others.

The Radiative Transfer model for Television Infrared Observation Satellites Operational Vertical Sounder (RTTOV) is designed for operational usage as a fast radiative transfer scheme (Saunders et al., 1999). In previous versions (RTTOV-8 and older), the Zeeman effect was included as transmission offsets based on Liebe (1981) but

AMTD
8, 10179–10211, 2015

Kobayashi et al. (2009) showed that this scheme introduced unacceptable errors for retrievals of atmospheric parameters. It was concluded that the old method for Zeeman effect calculations in RTTOV is worse for assimilations than simply ignoring the Zeeman effect altogether. This is problematic as the uppermost atmospheric levels are the least constrained part of the numerical weather prediction models. The errors at the uppermost regions of the numerical weather prediction profiles can be ∼ 5 K, with the top-of-the-profile having even larger errors of up to 10 or 20 K, but the magnitude of the errors depend on latitude and season. Inaccurate modeling of the radiation from these parts of the profile does not help to constrain the temperatures enough in the assimilation schemes. A new and fast Zeeman effect radiative transfer scheme designed by Han et al. (2007, 2010) has been implemented in RTTOV since version 10.

The Atmospheric Radiative Transfer Simulator (ARTS) is designed to be a reference radiative transfer model (Buehler et al., 2005; Eriksson et al., 2011). The ARTS Zeeman module implementation is described by Larsson et al. (2014) and has been validated by Navas-Guzmán et al. (2015). This work focuses on comparing ARTS with the new RTTOV scheme for the higher altitude SSMIS channels that are covered by numerical weather prediction profiles, and it is partly based on previous technical work presented by Larsson (2014). SSMIS is a conical scanner flying at an inclination of around 100° at about 800 km altitude. It is scanning with a sensor zenith angle of ∼ 50° relative to the surface and covers a 2200 km wide swath ahead of the satellite. For the upper atmospheric sounding channels that we are interested in, the swath is divided into 30 pixels with approximately 25 ms integration time each. Between scans, SSMIS use what remains of its 1.9 s scan cycle to calibrate against hot and cold loads. Model comparisons as this have proven valuable in the past for other spectral regions (see Buehler et al., 2006), as they allow us to quantify differences between the fast and the reference model schemes. Besides for numerical weather prediction applications, it is also important to quantify model discrepancies for climatological studies, where statistical methods are used to identify trends that can be small compared to an individual measurement's noise equivalent brightness temperature.

AMTD
8, 10179–10211, 2015

The next section describes the way both models handle the Zeeman effect, and it also describes how we conduct our comparison. Later sections present the model comparisons, and conclude this work with some remarks on future prospects.

2 Method

We focus our efforts on SSMIS channels 19 through 22, which are sensitive to circular polarization of four O_2 lines between 60 and 64 GHz, and have weighting functions with peaks that range in altitudes between 40 and 80 km (see Han et al., 2007). For each channel we have prepared five sets of brightness temperature data. One of these sets are measurements from SSMIS onboard DMSP-18 taken on 25 September 2013 between midnight and six in the morning (UTC). The other four datasets are forward simulations in ARTS and RTTOV using the atmospheric profiles derived by Met Office's numerical weather prediction for the SSMIS measurements. The four simulated sets are (1) ARTS with a three-dimensional magnetic field, (2) RTTOV with a two-dimensional magnetic field (i.e. independent of altitude), (3) ARTS with the same two-dimensional magnetic field as RTTOV, and (4) ARTS without any magnetic field at all. The following subsections describe necessary components of our forward simulations and discuss a few error sources when comparing the datasets to one-another.

2.1 Model descriptions

This subsection describes how the models treat the Zeeman effect. Sources to the broader transfer schemes are cited, but not reviewed in detail.

2.1.1 RTTOV

RTTOV is a fast radiative transfer model used in numerical weather prediction data assimilation schemes. It achieves its speed by pre-calculations of coefficients for several predictors, based on a training set of monochromatic transmittances, that translate

AMTD
8, 10179–10211, 2015

the atmospheric profiles into polychromatic transmission for select channels at some atmospheric profile levels. Coefficients for these predictors have been determined for many operational instruments, and the model is widely used. The transmission is used to calculate the sensor-measured intensity using

$$I = \sum_{i}^{n} B(T_i, f_0)\Delta\tau_i(\cdots), \tag{1}$$

where the index i is for each simulated layer of the atmospheric profile, n is the number of layers constructed from the profile, $B(T_i, f_0)$ is the Planck function for the center of the polychromatic channel, T_i is the temperature of the ith layer, and $\Delta\tau_i(\cdots)$ is the difference in the transmission to space across the layer. The triple dots indicates inputs to the transmission prediction scheme. For more information on the predictors, see Saunders et al. (1999).

There is no polarization in RTTOV as it models scalar radiative transfer. However, in deriving the RTTOV coefficients, the polarized nature of the Zeeman effect (and of other effects) is dealt with in monochromatic calculations of the polarization state of the entire transmission. The output of these calculations is the coefficients for the polarization component that is relevant for the polychromatic channel. The effective transmission from a level is thus

$$\tau_{x,i} = \mathbf{P}_{i+1}\mathbf{P}^{\dagger}_{i+1}\Big|_{x}, \tag{2}$$

where † indicates the conjugate transpose of the matrix, x indicates evaluation for the transmission of the wanted polarization component, and, counting upwards along the radiation path,

$$\mathbf{P}_i = \mathbf{T}_n\mathbf{T}_{n-1}\mathbf{T}_{n-2}\cdots\mathbf{T}_i, \tag{3}$$

where $\mathbf{T}_i$ is the polarized transmission across the ith level. For Eq. (1), $\Delta\tau_i = \tau_{i+1} - \tau_i$. The transmission from the $n+1$ level is taken as unity when considering $\Delta\tau_n$. The work

AMTD
8, 10179–10211, 2015

by Han et al. (2007) discusses the Zeeman implementation in detail and gives the predictors (in their Table 2). RTTOV uses a two-dimensional magnetic field consisting, for the entire radiation path, of just one magnetic field magnitude and one angle relative to the viewing direction of the instrument. These magnetic parameters are combined with the layer temperature to form the predictors.

2.1.2 ARTS

ARTS is a monochromatic line-by-line radiative transfer model that calculates absorption from a spectral line database for every level of the atmospheric profile. The intensity as seen by a simulated sensor in ARTS is from solving

$$\boldsymbol{I}_{\text{out}} = \exp\left[-\mathbf{K}_i r_i\right] \boldsymbol{I}_{\text{in}} + \left(\mathbf{1} - \exp\left[-\mathbf{K}_i r_i\right]\right) \boldsymbol{B}(T_i, f) \tag{4}$$

for each layer, where $\mathbf{K}_i$ is the polarized propagation matrix for the ith layer, r_i is the distance the radiation transfers through the layer, $\boldsymbol{I}_{\text{in}}$ is the incoming polarized radiation, and $\boldsymbol{B}(T_i, f)$ is the source function column vector (here $[B(T_i, f),\ 0,\ 0,\ 0]^{\mathrm{T}}$, where $B(T_i, f)$ is the Planck function). For details on the ARTS calculations see Eriksson et al. (2011).

The Zeeman module of ARTS calculates the Zeeman-affected propagation matrix at every atmospheric level by splitting lines into their polarized components as a function of the local magnetic field orientation. The propagation matrices are then averaged over the layer and used in Eq. (4). Both three-dimensional and two-dimensional magnetic fields are accepted as input. If the magnetic field is three-dimensional this means that there is a unique magnetic vector per level, whereas the two-dimensional magnetic field is similar to the RTTOV definition. In either case, ARTS keeps the polarization of the propagation matrices stored throughout the modeled transfer. By the end of the simulation, the polarized polychromatic sensor response is calculated from the monochromatic simulations and the channels' spectral responses. For more details on the ARTS Zeeman module see the work by Larsson et al. (2014). Navas-Guzmán et al. (2015) recently and successfully simulated ground-based observations of molecular

AMTD
8, 10179–10211, 2015

oxygen microwave radiation using the ARTS Zeeman module for several observational directions at high spectral resolution, which validates the ARTS implementation of the Zeeman effect for linear polarization.

2.2 The atmospheric profile inputs

There were a total of 8300 atmospheric profiles used for the simulations in this work. The profiles are derived from Met Office's numerical weather prediction model. For a description of the Met Office numerical weather prediction profiles at high altitude and a list of assimilated data, see Long et al. (2013). The profiles are abstractly shown in Fig. 1. Note that there is an unfortunate visual illusion in Fig. 1 that there is a discontinuity between the temperature at the 10 Pa level and the temperature at higher pressure levels. One major problem we encounter is that the channels of SSMIS are sensitive to altitudes that are above the numerical weather prediction profiles' top at 10 Pa. The weighting functions of channels 21 and 22 are mostly covered by the 10 Pa level but the weighting functions of channels 19 and 20 are not covered. To work around the problem of insufficiently high-reaching pressure levels of the Met Office profiles, we assume that all higher altitude pressure levels have the same temperature as the 10 Pa level. This assumption is simple and inaccurate, as the lapse rates at high altitudes are generally large, but it is another work altogether to define how to deal with the temperature field above the top of the numerical prediction profiles in a way that minimizes errors. One reason to use a constant temperature extrapolation for this work follows from that RTTOV predicts optical depths on pre-set coefficient levels. When presented with an atmosphere having insufficiently high-reaching pressure levels, RTTOV does this after assigning the temperature of the supplied atmospheric top to all the overlying coefficient levels, which is an extrapolation at constant temperature across the overlying layer of gas. The radiative transfer integration is performed subsequently on the supplied levels, but includes the source function and the absorption for the overlying layer of gas by, in effect, moving the supplied top at fixed temperature across this layer to represent the space boundary. Since the radiation of both channels 21 and 22 is

AMTD
8, 10179–10211, 2015

mostly emitted at an altitude range covered by the Met Office atmospheric profiles, forcing a constant temperature above the top emulates the behavior of RTTOV when it is directly supplied with the Met Office profiles for these channels. This still means that the simulated results of channels 19 and 20 are unrealistic. We therefore favor the low altitude channels 21 and 22 in this comparison work but include a brief discussion on how the models differ for the higher channels 19 and 20. This discussion focus on qualitative differences between the models that are apparent for the channels despite the otherwise unrealistic simulations. As one more note on the atmospheric profiles, we assume, for simplicity, that there is a constant molecular oxygen volume mixing ratio for the entire profile even though this is not the case above ~ 80 km.

Version 11 of the International Geomagnetic Reference Field (IGRF-11; Finlay et al., 2010) is used for the ARTS simulations with a three-dimensional magnetic field. The two-dimensional magnetic field values at the altitude corresponding to 5 Pa have been extracted from IGRF-11 for both ARTS and RTTOV for those simulations. These extracted values are mapped in Fig. 2, which also shows the global coverage of the datasets. The argument for using a two-dimensional magnetic field is that the magnetic field does not change much along the path of a transfer. If this argument is good for SSMIS observations, then the difference in brightness temperature as a function of magnetic field extraction altitude will be small for the simulations.

2.3 Spectroscopic considerations

The RTTOV simulations have been performed with the prediction coefficients derived by Han et al. (2007) in this study. ARTS uses line center frequencies from the Jet Propulsion Laboratory spectroscopy database (http://spec.jpl.nasa.gov/). There is a mismatch between the input line centers to ARTS and RTTOV by exactly 8.4, 8.1, 8.9, and 8.2 kHz referring to Table 1 in Han et al. (2007) for the 7+, 9+, 15+, and 17+ O_2 lines, respectively. ARTS always uses the higher frequency. The line centers given by, e.g., Tretyakov et al. (2005) are 2.2, 1.9, 5.1, and 7.4 kHz below the line centers used by ARTS, but were derived for use at low altitudes where pressure broadening is more

AMTD
8, 10179–10211, 2015

important than exactness of line centers. Nevertheless the model input spectroscopy is similar and should be compared with the frequency stability of SSMIS reported by Kunkee et al. (2008) (80 kHz for channels 19, 20, and 21; 120 kHz for channel 22). Since the frequency instabilities are larger than differences in the lines' central frequencies between the models, we do not think that line center accuracy is crucial for the comparison with SSMIS data, but it can still introduce biases between the models. The channels' spectral response and a few examples of the simulated spectra from ARTS can be seen in Fig. 3. (Note that from code review at the Met Office for the derivation of RTTOV's coefficients, we find that it appears that round-off levels of 100 kHz have been used for the line centers. The resulting differences in line centers between ARTS and RTTOV are still small compared to SSMIS frequency stability. They are instead 16, 32, 14, and −26 kHz for the 7+, 9+, 15+, and 17+ lines, respectively.)

From Fig. 3, we see that channels 19 and 20 are in the center of the broadened lines, and that channels 21 and 22 are in the line shape's wings near the equator (weak magnetic field strengths), but that channel 21 is on the edge of the strongly Zeeman-affected part of the line when the magnetic field is stronger (i.e., near the poles). It is clear from this figure in combination with Fig. 2 that the increased magnetic field strength at higher latitudes causes a stronger broadening of the line. Since the SSMIS channels measure so close to the line centers, resulting errors from line center mismatches have been studied using the same simulations as shown in Fig. 3. The results of these tests are in Fig. 4, which shows ARTS simulations with uniformly shifted line centers (emulating a channel frequency shift). We see that the effect of the channel frequency shift is large for channels 19 and 20 near the equator ($\Delta T_b \approx \pm 2$ K at ±50 kHz shift looking westward) and that the effect here strongly depends on the observational geometry ($\Delta T_b \approx \mp 2$ K at 50 kHz shift when instead looking eastward). Closer to the north pole, the effect is still noticeable but is fairly constant with observational geometry ($\Delta T_b \approx -0.1$ K at ±50 kHz). There is a noticeable effect on channel 21 of $\Delta T_b \approx \pm 0.5$ K at ±50 kHz for the polar simulations and $\Delta T_b \approx \pm 0.2$ K at ±50 kHz for equatorial simulations. Channel 22 is only weakly affected by a shifting channel center,

AMTD
8, 10179–10211, 2015

with $|\Delta T_b| < 0.05$ K even at ±150 kHz shift. Note that Figs. 3 and 4 only represent two locations on the globe and that the absolute effect of a shifting channel center changes over the globe.

2.4 Are there layering issues?

Since ARTS averages optical properties and RTTOV averages atmospheric properties to create the layer transfer, we must quantify the errors introduced by this model discrepancy. We do this by artificially decreasing the maximum layer thickness (r_i of Eq. 4) for ARTS. We find that using an atmospheric layering of 50 m for a few of the profiles instead of using the same layering thickness as RTTOV changes our results by only $\sim 2 \times 10^{-4}$ K. The layering thickness is therefore not an issue for ARTS. We cannot test this for RTTOV directly without altering the predictor coefficients, but it is shown by Han et al. (2007) that using a sparsely layered approach or using a 1 km altitude grid does not alter the simulated brightness temperature by much. From these observations we argue that there is no issue with the layers in the present study.

3 Results and discussions

The results of our comparison are summarized in Table 1. Channel-by-channel, the table shows the mean differences between the compared datasets, their corresponding standard deviations, and the channels' noise equivalent temperatures. Figures 5 to 8 show the datasets in spread plots and as global distribution maps for channels 19–22. Figure 9 shows SSMIS measurements cf. the simulations for channel 21, and Fig. 10 shows SSMIS measurements cf. the simulations for channel 22.

AMTD
8, 10179–10211, 2015

3.1 Model to model

3.1.1 Channels 19 and 20

Figure 5 shows the Channel 19 comparison of RTTOV with ARTS, which was run using both a full three-dimensional magnetic field and an identical two-dimensional magnetic field setup as used by RTTOV. From Table 1, it can be seen that the mean brightness temperature differences between the models are small on average regardless of magnetic field setup, with both comparisons mean difference showing $|\Delta T_b| < 0.34$ K. This is about the same size as the average Zeeman effect in ARTS at $\Delta T_b \approx -0.44$ K. (We determine the brightness temperature influence of the Zeeman effect by turning the magnetic field off in ARTS and compare the resulting simulations with the ARTS simulations that use a three-dimensional magnetic field.) There is a large increase in the standard deviation of the differences from 0.33 K in the two-dimensional magnetism comparison to three-dimensional magnetism comparison, which has standard deviation of 1.8 K. There is a still larger increase in standard deviation to 2.9 K if the Zeeman effect is ignored.

From the global distribution maps shown in Fig. 5, we see that the largest discrepancies for channel 19 between RTTOV and ARTS with three-dimensional magnetism are located all across the equator, with brightness temperature differences of up to 7 K systematically distributed in higher and lower brightness temperature regions; most warmer regions are to the south of the equator and most colder regions are to the north of the equator when the satellite is moving southward. When the satellite is moving northward, the resulting warm-cold region distribution seems to change across the swath. By remembering Fig. 2, which shows the two-dimensional magnetic field, we can by eye correlate these larger brightness temperature differences with areas of relatively weak magnetic field strength and with a magnetic field angle that is close to parallel with the radiation path. Thus, if the the satellite had been moving northward over Eurasia, instead of over the Pacific ocean, we cannot expect to see the same

AMTD
8, 10179–10211, 2015

type of regional discrepancies since the magnetic field angle is changed by the viewing geometry.

Looking only at the comparison of RTTOV and ARTS simulations with two-dimensional magnetism for channel 19, we still find brightness temperature differences between the models of up to 1 K. There appears to be a weak positive bias of around 0.5 K in the equatorial regions and a weak negative bias of around 0.6 K closer to the poles. We cannot identify the reason for these discrepancies clearly but suspect that the line center frequency differences of around 20 kHz between the models can explain some of these differences.

For channel 20 in Fig. 6, most of the same features are available as for channel 19 in Fig. 5, with a few modifications. From Table 1, the average brightness temperature differences between models are small, with both comparisons showing a mean of $|\Delta T_b| < 0.17$ K. The average model-to-model difference is thus much smaller than the average Zeeman effect in ARTS, which is at $\Delta T_b \approx -2.2$ K. The standard deviation of the model-to-model differences changes in the same way for channel 20 as it does for channel 19. RTTOV simulations minus ARTS simulations with three-dimensional magnetism have a much larger standard deviation of 1.7 K than the standard deviation of 0.27 K for RTTOV simulations minus ARTS simulations with two-dimensional magnetism. For channel 20 the ARTS Zeeman effect standard deviation of 2.0 K is relatively close to the largest model-to-model standard deviation. As for channel 19, there are systematic regional discrepancies of up to 7 K for channel 20 near the equator for RTTOV cf. three-dimensional magnetism ARTS simulations that mostly goes away when using two-dimensional magnetism in ARTS. Again, these regional discrepancies seem, at least partially, to be caused by the viewing geometry and the magnetic field angle, and are thus expected to be different when the satellite moves northward than when it moves southward.

The errors that remain in the comparison with RTTOV and ARTS simulations with two-dimensional magnetism for channel 20 are similar to those for channel 19 of up to ~ 1.5 K. Because both line centers for channel 20 are shifted in frequency with the

AMTD
8, 10179–10211, 2015

same sign, we can compare the remaining discrepancies in Fig. 6 to the channel frequency shift presented in Fig. 4. As a test not presented in any figures of this work, we ran ARTS with changed line center frequencies of 30 kHz for channel 20. This altered spectroscopy reduce the mean difference between the models by half, but the standard deviation still remains fairly unchanged. This means that there are still unidentified discrepancies between the models for channel 20.

3.1.2 Channels 21 and 22

Common to both the lower peaking channels 21 and 22 is that the reduction to two-dimensional magnetism in ARTS is numerically noticeable but much smaller than for channels 19 and 20. It is possible in Fig. 7, for channel 21, to see this difference qualitatively in the global distributions near magnetically strong regions. E.g., above Siberia there is a region where the ARTS simulations with two-dimensional magnetism are slightly warmer with $\Delta T_b \approx 0.1$ K to RTTOV, than the ARTS simulations with three-dimensional magnetism with $\Delta T_b \approx -0.2$ K to RTTOV. It is also possible to see a systematic 1 K gradient over the swaths near the equator in the comparison of RTTOV and three-dimensional ARTS. This gradient is gone in the comparison with the two-dimensional ARTS simulations. E.g., in the three-dimensional case above the Pacific Ocean, the brightness temperature differences change from $\Delta T_b \sim -2.5$ K to $\Delta T_b \sim -1.5$ K over the swath. However, in the two-dimensional case the same swath brightness temperature difference is a constant $\Delta T_b \sim -1.5$ K. As for channels 19 and 20, these swath discrepancies should change whether SSMIS is scanning northward or southward.

Focusing only on two-dimensional magnetism simulations for channel 21 (Fig. 7; right column), the polar regions agree fairly well between ARTS and RTTOV, with $|\Delta T_b| < 0.6$ K, barring a -1 K region above Antarctica close to 0° E longitude. These < 0.6 K differences are possible to understand from the 30 kHz line shifts identified for channel 20 above. As for channel 20, however, introducing the line center shifts only reduces the model-to-model discrepancies, without much change in the standard deviation. (We re-

AMTD
8, 10179–10211, 2015

mind the reader that channels 20, 21, and 22 measure the same two lines as is shown in Fig. 3 so that effects on one of the channels should be similar in the others.) The largest differences between the models are found across the equator with maximum differences of $\Delta T_b \approx -3$ K. We cannot explain these large differences from the channel shifts of Fig. 4. The standard deviation of the model-to-model difference is about 0.56 K. In relation to the sensor noise equivalent temperature of 1.9 K, the model-to-model standard deviation is small. The mean difference between the models should be compared to the size of the Zeeman effect for channel 21 at $\Delta T_b = -3.1$ K, which is the largest average Zeeman effect for all of the channels. From this comparison, the mean difference between the models is also small.

For channel 22, there seems to be no correlation between magnetic field parameters and model-to-model differences. This is not surprising considering that the Zeeman effect is not very important, with an average effect of $\Delta T_b = 0.13$ K that has a standard deviation of only 0.088 K. The mean differences between the models are $\Delta T_b \approx -0.53$ K with a standard deviation of 0.24 K, regardless of magnetic field setup in ARTS. As for channel 21, we find that near the equator there is a larger than average negative bias of $\Delta T_b \approx -0.75$ K. Another region of interest is the south pole, where the largest model-to-model differences occur – not shown in any plots is that the Antarctica is the warmest region in our simulations with atmospheric temperature of around 280 K for channel 22. From the scatter plots of Fig. 8, we see that there are beginnings of deviation between the models at higher temperatures, which shows the Antarctica deviations. One potential cause for these discrepancies is therefore that the RTTOV coefficients were derived using transmission coefficients from simulations with an atmospheric training set that also had highest temperatures around 280 K at the peak of the weighting function of channel 22. That RTTOV coefficients derived for atmospheric input close to the limits of the training set can cause accuracy issues in RTTOV has previously been identified as a problem by Buehler et al. (2006) for water spectroscopy models. In other regions, the model-to-model differences are small and appears to oscillate around 0 K.

AMTD
8, 10179–10211, 2015

3.2 Models to measurements

Direct comparison of simulated measurements with the SSMIS dataset is only possible for channels 21 and 22 because the higher altitude channels 19 and 20 are not covered by the altitude levels of the numerical weather prediction profiles. We want to remind the reader that the Met Office numerical weather prediction model profiles are believed to be inaccurate at higher altitudes. All such inaccuracies are retained in the following comparisons of models to measurements.

The comparisons for channel 21 between SSMIS measurements, with regards to RTTOV simulations and with regards to ARTS simulations with three-dimensional magnetism, are found in Fig. 9. We find that the mean value of SSMIS measurements minus RTTOV simulations is −1.3 K, and the mean value of SSMIS measurements minus ARTS simulations is −0.34 K. ARTS agrees better with SSMIS than RTTOV. Both comparisons have a standard deviation of around 2.4 K, and the noise equivalent temperature of the sensor is 1.9 K (Kunkee et al., 2008). So even if ARTS appears to be better, RTTOV simulations are close to SSMIS measurements given the sensor's noise and RTTOV is close to ARTS given the simulations to measurement standard deviations.

One key point that we want to take note of is that the noise of channel 21 is always smaller than the standard deviation of simulations to measurement. This is a similarity between our study and the one performed by Han et al. (2007). They found that RTTOV agrees with SSMIS at a root mean square of 2.3 K at a mean difference of −0.95 K for channel 21. Han et al. use retrieved temperature profiles by the limb-scanning SABER instrument on-board the TIMED satellite. This should mean that their temperature profiles are reasonably accurate, since limb-scanners have a high signal to noise ratio. Still, they found, as we do, that the standard deviation of the simulations to measurement are consistently larger than the noise of the sensor.

Looking in more details at the global distribution maps, we see that the largest discrepancies for both models are available closer to the poles, with a tendency for warmer

AMTD
8, 10179–10211, 2015

brightness temperature differences (up to about 7 K) in the south and colder brightness temperature differences in the north (down to about −7 K). The weighting function of channel 21 is shifted upwards for stronger magnetism (Han et al., 2007). This upwards shift places a significant part of the weighting function at pressure levels where we have set the temperature to a constant value (above the 10 Pa level). Clearly a better method for extending the temperatures above 10 Pa is required. Across the equator the models are closer to SSMIS measurements. RTTOV agrees better with SSMIS measurements near the equator, with an average difference of around −1 K, than ARTS simulations, which has an average difference of 2 K to the SSMIS measurements.

There are some similarities between the channel 21 and the channel 22 comparisons of model simulations and SSMIS measurements as found in Fig. 10. In average, ARTS still agrees better than RTTOV with SSMIS measurements, with the respective differences to measurements being $\Delta T_b \approx -0.63$ K for ARTS and $\Delta T_b \approx -1.3$ K for RTTOV as seen in Table 1. Both models have approximately 1.4 K standard deviation to the measurements, which is similar to the sensor equivalent noise temperature of 1.3 K (Kunkee et al., 2008). Since the model-to-measurement standard deviation retains atmospheric input errors, this means that the models have a good agreement with the measurements. There are still a few dominating features visible in the global distribution maps. These features are all in the Southern Hemisphere, with a region above West Antarctica that has a −7.5 K bias compared to both models, and two regions with a 3 K bias to the observations, one located just north of the cold Antarctica anomaly and another located towards the east of it.

We note that RTTOV and SSMIS agree better for channel 22 in our study than in the study by Han et al. (2007). They found approximately the same average difference between RTTOV and SSMIS as we did ($\Delta T_b \approx -1.3$ K), but the standard deviation in their test was much larger at 2.2 K compared to ours of 1.4 K. The temperature profiles are more accurate for limb sounding, so their uncertainties should reasonable be below or similar to ours. One possible explanation is that there are measurements with colder brightness temperatures included in the study by Han et al. (2007) than in our study.

AMTD
8, 10179–10211, 2015

These lower brightness temperatures were consistently underestimated by RTTOV, which should increase the standard deviation.

4 Summary, conclusions and outlook

We have presented a comparative study showing how well the fast RTTOV agrees with reference model ARTS for the high altitude channels 19–22 of SSMIS using globally distributed numerical weather prediction model profiles from Met Office. This study shows that the RTTOV Zeeman effect scheme for SSMIS implemented by Han et al. (2007) works well. The agreements between the forward simulations and the corresponding SSMIS measurements is generally good but there are some discrepancies; quantitative values of the comparison are summarized in Table 1.

We conclude, when comparing ARTS to RTTOV, that using a three-dimensional magnetic field in ARTS gives an increased standard deviation compared to using a two-dimensional magnetic field in ARTS for channels 19 and 20; this increase is from 0.3 to 1.8 K for channel 19 and from 0.27 to 1.7 K for channel 20. The brightness temperature differences by a three-dimensional magnetism for these channels is found to be up to ±7 K across the equator, whereas ARTS with a two-dimensional magnetic field is in the range ±1.5 K from RTTOV. Similar brightness temperature differences between two- and three-dimensional magnetism for channel 21 exists but they are much smaller in magnitude. In regions where the magnetic field is strong (closer to the poles), the dimensionality of the magnetic field can give differences of about 0.5 K in local regions. Closer to the equator, the differences occur over a swath of measurement and are found to be about 1 K large. A large part of the discrepancies caused by switching between two- and three-dimensional magnetism is due to observational geometry; a satellite moving northward and one moving southward will see different magnetic angles of a region and thus experience a different regional discrepancy pattern. Channel 22 is unaffected by this problem. We also find that the differences between ARTS simulations using two-dimensional magnetic fields and ARTS simulations using

AMTD
8, 10179–10211, 2015

three-dimensional magnetic fields are smaller than the differences between ARTS and RTTOV for channels 21 and 22. We have identified model brightness temperature differences for channel 21 of about 3 K across the equator that we cannot explain from this study. For channel 22 there is also an unexplained brightness temperature difference across the equator of −0.75 K. There seems to be a limit in the temperature range for RTTOV's training data that lowers RTTOV accuracy at the highest atmospheric temperatures above the Antarctica, creating a model-to-model bias of about 1 K for regions with the highest atmospheric temperature in this study.

Our results imply that RTTOV, with the new Zeeman scheme by Han et al. (2007), models the SSMIS dataset within acceptable accuracy compared to sensor noise parameters. This in turn shows that the concerns Kobayashi et al. (2009) raised on using RTTOV's past Zeeman capabilities for data assimilation schemes are addressed. We recommend that future iterations of numerical weather prediction software starts using versions of RTTOV from version 10 and onwards for the assimilation of SSMIS channels 21 and 22. It is likely that model discrepancies for channel 21 would be reduced if the model top levels reached higher altitudes; a level top at 100 km is also necessary for channels 19 and 20 to be modeled and assimilated. It would also be better to use a three-dimensional magnetic field in RTTOV than a two-dimensional magnetic field but such a Zeeman scheme is not available yet. An option today is to apply biases, similar to those we find between ARTS and RTTOV in this work, to correct the simulated measurements in the assimilation schemes. Especially regional biases have to be described for the inversions. Uncertainties in the atmospheric temperature field of the numerical weather prediction model levels at high altitude are nevertheless large today and consideration of the higher altitude SSMIS channels can help mitigate these uncertainties.

As an outlook, there is an ongoing effort to use ARTS for retrievals of atmospheric temperature profiles using all of the high altitude SSMIS channels. The results of these efforts will be reported upon in a future work.

AMTD
8, 10179–10211, 2015

Acknowledgements. This work was partly funded by EUMETSAT grant number NWP_VS13_02, with report number NWPSAF-MO-VS-049. The writing of this article mainly took place in Hamburg under CliSAP stipend. The authors also want to acknowledge the communities that support, both by usage and development, the two radiative transfer simulators.

References

Anderson, G. P., Clough, S. A., Kneizys, F. X., Chetwynd, J. H., and Shettle, E. P.: AFGL atmospheric constituent profiles (0–120 km), Tech. rep., AFGL, Hanscom Air Force Base, Massachusetts, USA, TR-86-0110, 1986. 10181

Buehler, S. A., Eriksson, P., Kuhn, T., von Engeln, A., and Verdes, C.: ARTS, the atmospheric radiative transfer simulator, J. Quant. Spectrosc. Ra., 91, 65–93, 2005. 10182

Buehler, S. A., Courcoux, N., and John, V. O.: Radiative transfer calculations for a passive microwave satellite sensor: comparing a fast model and a line-by-line model, J. Geophys. Res., 111, D20304, doi:10.1029/2005JD006552, 2006. 10182, 10193

Eriksson, P., Buehler, S. A., Davis, C. P., Emde, C., and Lemke, O.: ARTS, the atmospheric radiative transfer simulator, Version 2, J. Quant. Spectrosc. Ra., 112, 1551–1558, 2011. 10182, 10185

Finlay, C. C., Maus, S., Beggan, C. D., Bondar, T. N., Chambodut, A., Chernova, T. A., Chulliat, A., Golovkov, V. P., Hamilton, B., Hamoudi, M., Holme, R., Hulot, G., Kuang, W., Langlais, B., Lesur, V., Lowes, F. J., Lühr, H., Macmillan, S., Mandea, M., McLean, S., Manoj, C., Menvielle, M., Michaelis, I., Olsen, N., Rauberg, J., Rother, M., Sabaka, T. J., Tangborn, A., Tøffner-Clausen, L., Thébault, E., Thomson, A. W. P., Wardinski, I., Wei, Z., and Zvereva, T. I.: International geomagnetic reference field: the eleventh generation, Geophys. J. Int., 183, 1216–1230, 2010. 10187

Han, Y., Weng, F., Liu, Q., and van Delst, P.: A fast radiative transfer model for SSMIS upper atmosphere sounding channels, J. Geophys. Res., 112, D11121, doi:10.1029/2006JD008208, 2007. 10181, 10182, 10183, 10185, 10187, 10189, 10194, 10195, 10196, 10197

Han, Y., van Delst, P., and Weng, F.: An improved fast radiative transfer model for special sensor microwave imager/sounder upper atmosphere sounding channels, J. Geophys. Res., 115, D15109, doi:10.1029/2010JD013878, 2010. 10182

AMTD

8, 10179–10211, 2015

Hartmann, G. K., Degenhardt, W., Richards, M. L., Liebe, H. J., Hufford, G. A., Cotton, M. G., Belivacqua, R. M., Olivero, J. J., Kämpfer, N., and Langen, J.: Zeeman splitting of the 61 Gigahertz Oxygen (O_2) line in the mesosphere, Geophys. Res. Lett., 23, 2329–2332, 1996. 10181

Kobayashi, S., Matricardi, M., Dee, D., and Uppala, S.: Toward a consistent reanalysis of the upper stratosphere based on radiance measurements from SSU and AMSU-A, Q. J. Roy. Meteor. Soc., 135, 2086–2099, 2009. 10181, 10182, 10197

Kunkee, D. B., Poe, G. A., Boucher, D. J., Swadley, S. D., Hong, Y., Wessel, J. E., and Uliana, E. A.: Design and evaluation of the first special sensor microwave imager/sounder, Geosci. Remote Sens., 46, 863–883, doi:10.1109/TGRS.2008.917980, 2008. 10181, 10188, 10194, 10195, 10201

Larsson, R.: The Zeeman effect implementation for SSMIS in ARTS v. RTTOV, Tech. rep., EUMETSAT, Darmstadt, Germany, nWPSAF-MO-VS-049, 2014. 10182, 10203

Larsson, R., Buehler, S. A., Eriksson, P., and Mendrok, J.: A treatment of the Zeeman effect using Stokes formalism and its implementation in the Atmospheric Radiative Transfer Simulator (ARTS), J. Quant. Spectrosc. Ra., 133, 445–453, 2014. 10182, 10185

Lenoir, W. B.: Propagation of Partially Polarized Waves in a Slightly Anisotropic Medium, J. Appl. Phys., 38, 5283–5290, 1967. 10181

Lenoir, W. B.: Microwave Spectrum of Molecular Oxygen in the Mesosphere, J. Geophys. Res., 73, 361–376, 1968. 10181

Liebe, H. J.: Modeling attenuation and phase of radio waves in the air frequencies below 1000 GHz, Radio Sci., 16, 1183–1199, 1981. 10181

Long, D. J., Jackson, D. R., Thuburn, J., and Mathison, C.: Validation of Met Office upper stratospheric and mesospheric analyses, Q. J. Roy. Meteor. Soc., 139, 1214–1228, 2013. 10186

Navas-Guzmán, F., Kämpfer, N., Murk, A., Larsson, R., Buehler, S. A., and Eriksson, P.: Zeeman effect in atmospheric O_2 measured by ground-based microwave radiometry, Atmos. Meas. Tech., 8, 1863–1874, doi:10.5194/amt-8-1863-2015, 2015. 10182, 10185

Rosenkranz, P. W. and Staelin, D. H.: Polarized thermal microwave emission from oxygen in the mesosphere, Remote Sens., 23, 721–729, 1988. 10181

Rothman, L. S., Gordon, I. E., Babikov, Y., Barbe, A., Benner, D. C., Bernath, P. F., Birk, M., Bizzocchi, L., Boudon, V., Brown, L. R., Campargue, A., Chance, K., Cohen, E. A., Coudert, L. H., Devi, V. M., Drouin, B. J., Fayt, A., Flaud, J.-M., Gamache, R. R., Harrison, J. J., Hartmann, J.-M., Hill, C., Hodges, J. T., Jacquemart, D., Jolly, A., Lamouroux, J., Roy, R. J. L.,

AMTD
8, 10179–10211, 2015

Li, G., Long, D. A., Lyulin, O. M., Mackie, C. J., Massie, S. T., Mikhailenko, S., Müller, H. S. P., Naumenko, O. V., Nikitin, A. V., Orphal, J., Perevalov, V., Perrin, A., Polovtseva, E. R., Richard, C., Smith, M. A. H., Starikova, E., Sung, K., Tashkun, S., Tennyson, J., Toon, G. C., Tyuterev, V. G., and Wagner, G.: The HITRAN2012 molecular spectroscopic database, J. Quant. Spectrosc. Ra., 130, 4–50, 2013. 10181

Saunders, R., Matricardi, M., and Brunel, P.: An improved fast radiative transfer model for assimilation of satellite radiance observations, Q. J. Roy. Meteor. Soc., 125, 1407–1425, 1999. 10181, 10184

Schwartz, M. J., Read, W. G., and Van Snyder, W.: EOS MLS Forward Model polarized radiative transfer for Zeeman-split oxygen lines, IEEE T. Geosci. Remote, 44, 1182–1191, 2006. 10181

Stähli, O., Murk, A., Kämpfer, N., Mätzler, C., and Eriksson, P.: Microwave radiometer to retrieve temperature profiles from the surface to the stratopause, Atmos. Meas. Tech., 6, 2477–2494, doi:10.5194/amt-6-2477-2013, 2013. 10181

Tretyakov, M. Y., Koshelev, M. A., Dorovskikh, V., Makarov, D. S., and Rosenkranz, P. W.: 60-GHz oxygen band: precise broadening and central frequencies of fine-structure lines, absolute absorption profile at atmospheric pressure, and revision of mixing coefficients, J. Mol. Struct., 231, 1–14, 2005. 10187

Zeeman, P.: On the influence of magnetism on the nature of the light emitted by a substance, Astrophys. J., 5, 332–347, 1897. 10181

AMTD
8, 10179–10211, 2015

Table 1. Mean and standard deviations of our comparison for the four SSMIS channels. The left couple of columns with data are direct comparison between the SSMIS dataset and the corresponding full model simulations. The rightmost column is the Zeeman effect by turning the effect on-and-off in ARTS. The remaining columns compares RTTOV simulations with ARTS simulations using three-dimensional and two-dimensional magnetic fields. Noise levels are from Kunkee et al. (2008).

Channel		SSMIS cf. Full ARTS	SSMIS cf. RTTOV	RTTOV cf. 3-D mag. ARTS	RTTOV cf. 2-D mag. ARTS	Zeeman Effect
19	Mean	NA	NA	−0.336 K	−0.110 K	−0.435 K
	STD	NA	NA	1.8305 K	0.3304 K	2.8931 K
	Noise	2.7 K				
20	Mean	NA	NA	−0.068 K	0.1668 K	−2.244 K
	STD	NA	NA	1.7340 K	0.2679 K	1.9820 K
	Noise	2.7 K				
21	Mean	−0.344 K	−1.275 K	−0.931 K	−0.921 K	−3.125 K
	STD	2.4362 K	2.4462 K	0.5530 K	0.5676 K	1.8862 K
	Noise	1.9 K				
22	Mean	−0.628 K	−1.156 K	−0.528 K	−0.532 K	0.1285 K
	STD	1.3750 K	1.4023 K	0.2437 K	0.2428 K	0.0875 K
	Noise	1.3 K				

AMTD
8, 10179–10211, 2015

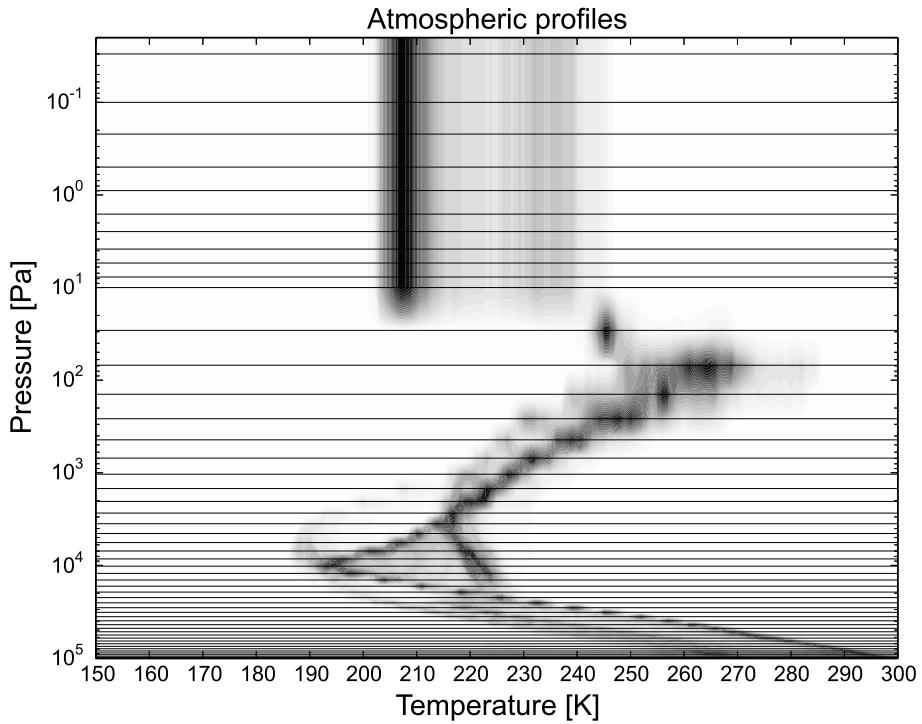

Figure 1. The atmospheric profiles used in this study. The horizontal lines are profile levels and color scale is normalized per profile level: darker regions in the figure indicates more profiles with that temperature.

AMTD
8, 10179–10211, 2015

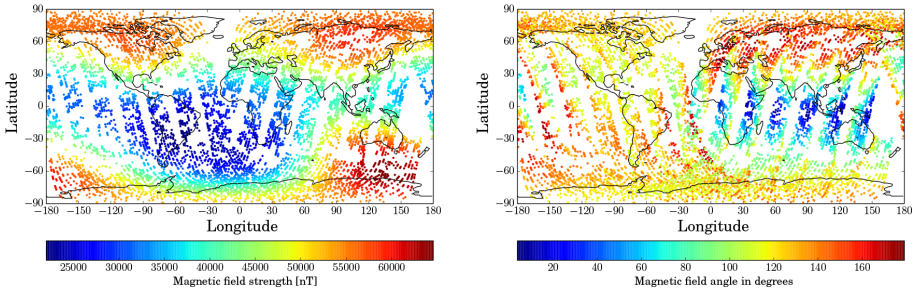

Figure 2. Magnetic field used in our simulation mapped on a two-dimensional surface showing the strength of the field in the left column. The right column contain the angle between the magnetic field vector and the radiation's propagation path. (This figure appears in Larsson, 2014, and is republished with rights from EUMETSAT.)

AMTD
8, 10179–10211, 2015

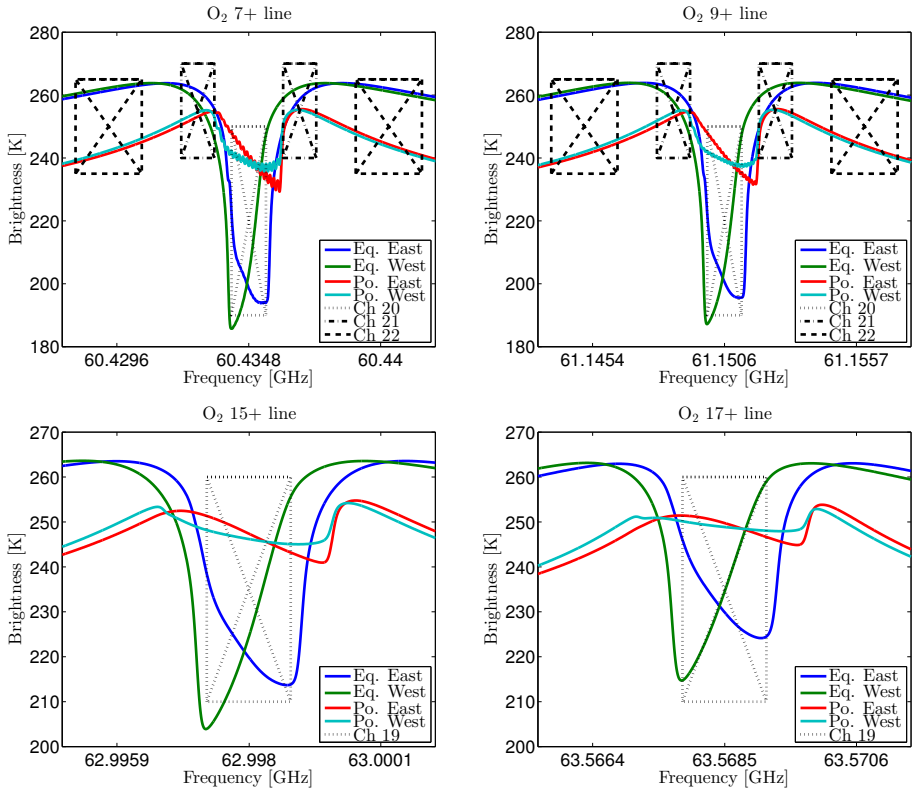

Figure 3. Channel configurations for SSMIS. The colors are for polar simulations (60° N 0° E; teal and red lines) and equatorial simulations (0° N 0° E; blue and green lines). The different colors are also the simulations azimuthal angle; blue and red responses have SSMIS looking towards the east (75°), whereas green and teal have it looking towards the west (−75°). The channels are indicated by black boxes of different line styles as seen in the legends. The simulated measurement response are assumed to be the average of the spectra within the frequency ranges.

AMTD
8, 10179–10211, 2015

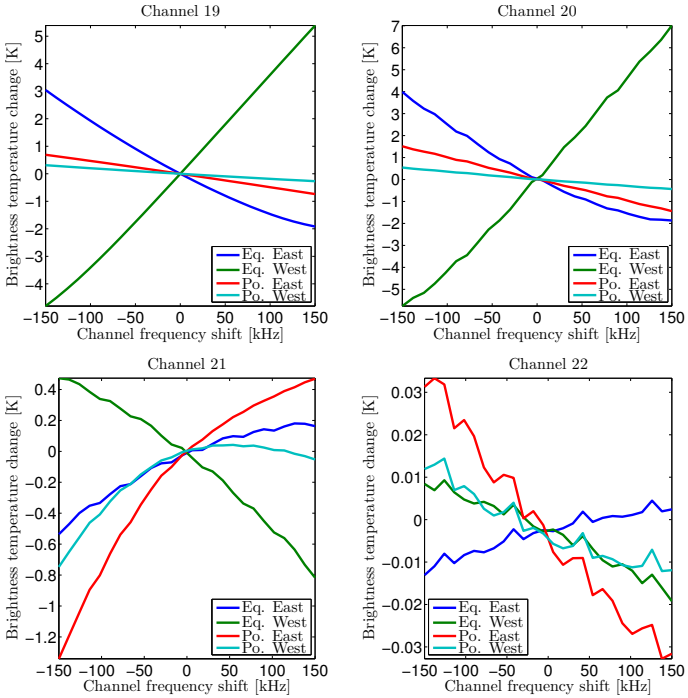

Figure 4. Changes in brightness temperatures introduced by an offset in channel frequency for a single atmospheric scenario. This figure shows the changes in channel brightness temperatures for the simulations in Fig. 3; both legends and line colors are for the cases in Fig. 3. The 0 kHz brightness temperature has been used as reference (hence 0 K at 0 kHz). The title of each subplot shows the channel.

AMTD
8, 10179–10211, 2015

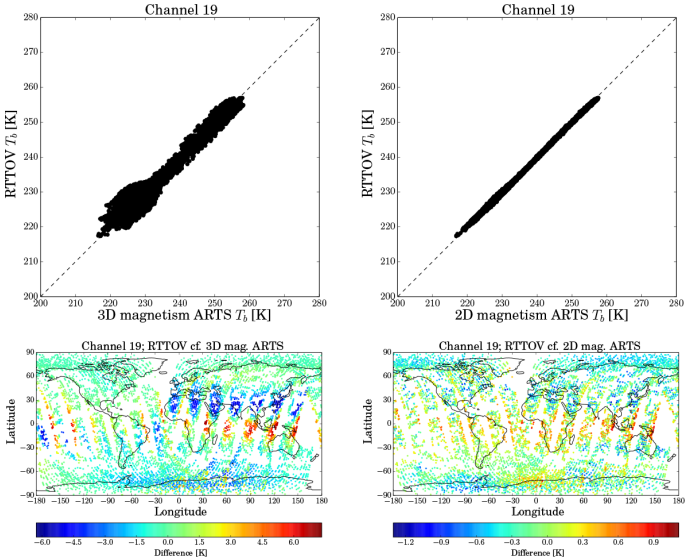

Figure 5. Channel 19 comparison of RTTOV and ARTS simulations. The upper row contains spread plots for RTTOV simulations on the *y* axis and for ARTS simulations on the *x* axis. The lower row contains the above spread plots mapped onto the surface of Earth to where the corresponding SSMIS measurement was done. In these maps, the magnitude of the difference between the simulations are shown in color. The color corresponds to ARTS minus RTTOV. The left column is RTTOV compared to ARTS simulations with three-dimensional magnetism and the right column is RTTOV compared to ARTS simulations with two-dimensional magnetism. It is important to note that the color scale changes between the maps; this has been done highlight all model differences, which are discussed in the text.

AMTD
8, 10179–10211, 2015

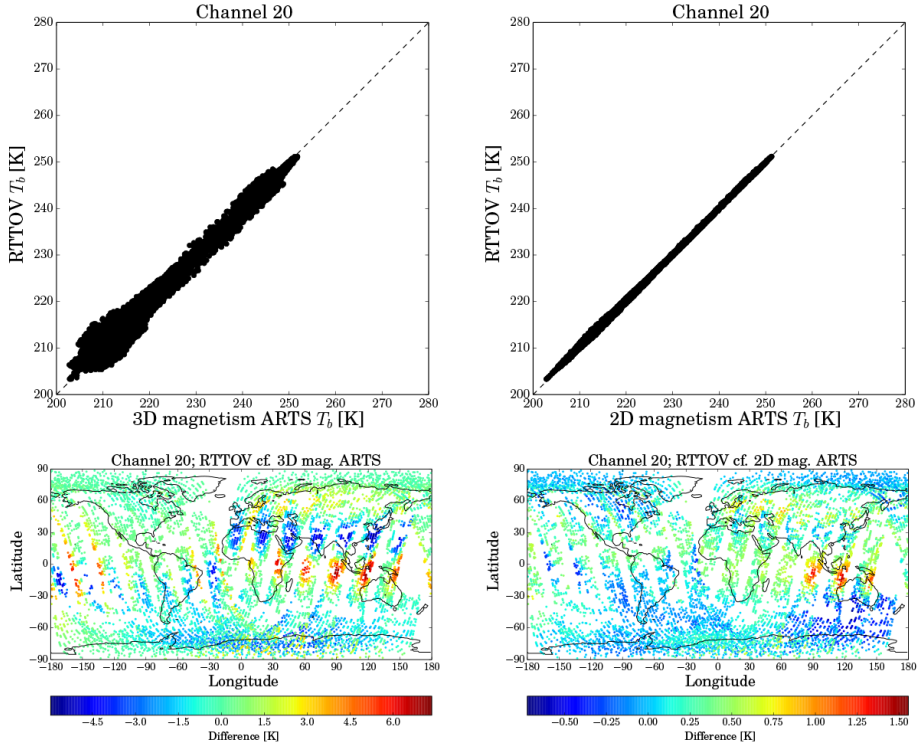

Figure 6. Channel 20 comparison of RTTOV and ARTS simulations as for Fig. 5.

AMTD
8, 10179–10211, 2015

High altitude SSMIS: radiative transfer model comparison for NWP

R. Larsson et al.

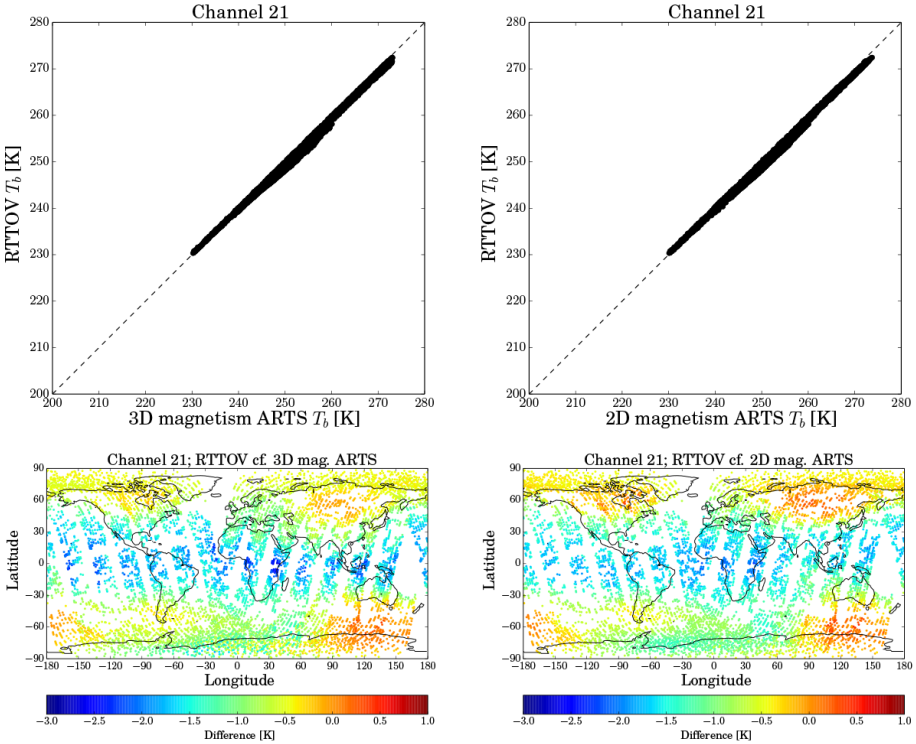

Figure 7. Channel 21 comparison of RTTOV and ARTS simulations as for Fig. 5 but with fixed color scale.

AMTD
8, 10179–10211, 2015

High altitude SSMIS: radiative transfer model comparison for NWP

R. Larsson et al.

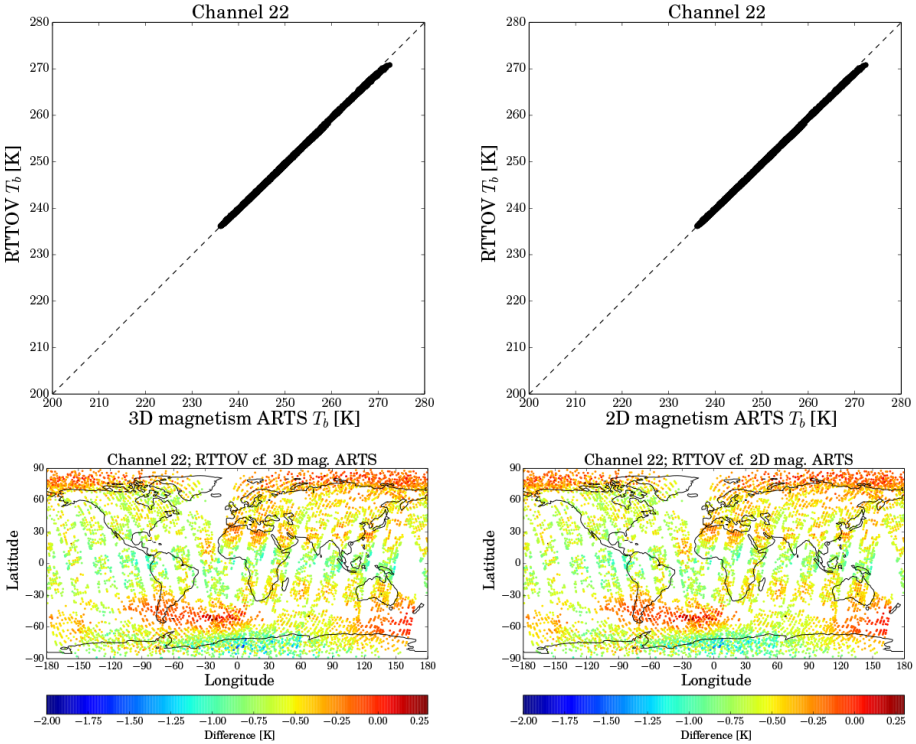

Figure 8. Channel 22 comparison of RTTOV and ARTS simulations as for Fig. 5 but with fixed color scale.

AMTD
8, 10179–10211, 2015

High altitude SSMIS: radiative transfer model comparison for NWP

R. Larsson et al.

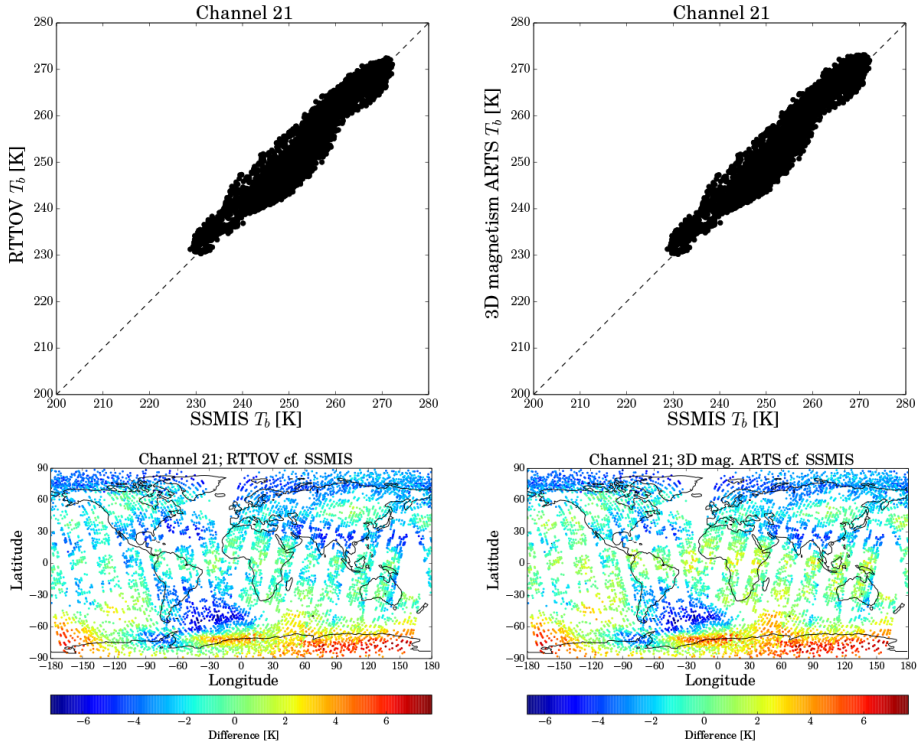

Figure 9. Comparison of model simulations and SSMIS measurements for channel 21. Similar to Fig. 5 with some changes. The left column spread plot still has RTTOV simulations on the *y* axis but SSMIS measurements on the *x* axis; the corresponding scatter map is for SSMIS minus RTTOV. The right column spread plot has ARTS simulations with three-dimensional magnetism on the *y* axis and SSMIS measurements on the *x* axis; the corresponding scatter map is for SSMIS minus ARTS.

AMTD
8, 10179–10211, 2015

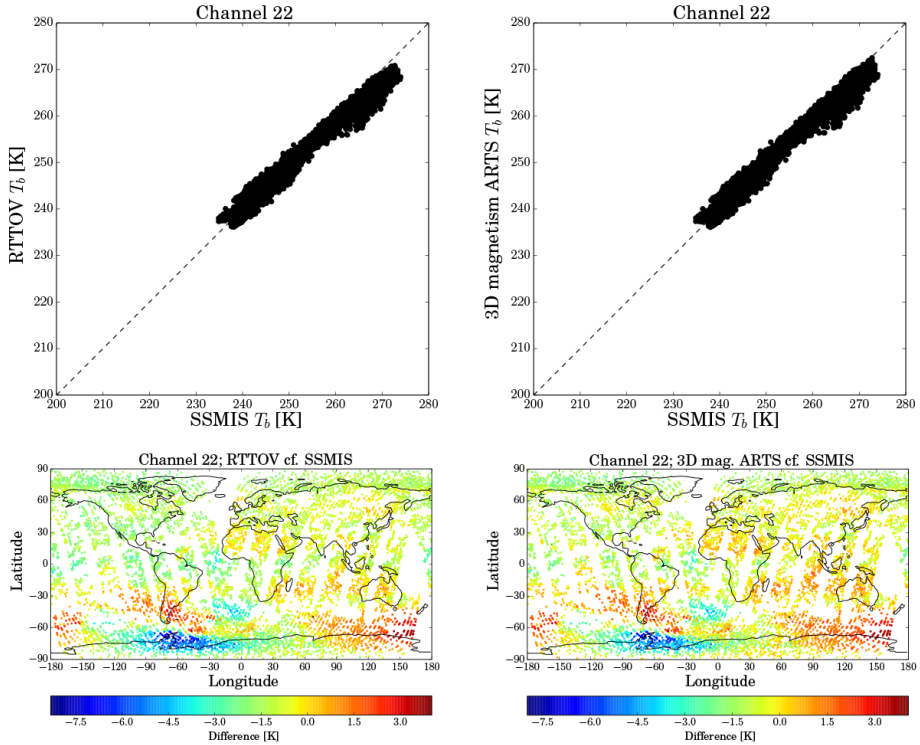

Figure 10. Comparison of model simulations and SSMIS measurements for channel 22 as for Fig. 9.

AMTD
8, 10179–10211, 2015

High altitude SSMIS: radiative transfer model comparison for NWP

R. Larsson et al.